nature structural & molecular biology

Dynamics and function of compact nucleosome arrays

Michael G Poirier[1,2], Eugene Oh[1], Hannah S Tims[1] & Jonathan Widom[1]

The packaging of eukaryotic DNA into chromatin sterically occludes polymerases, recombinases and repair enzymes. How chromatin structure changes to allow their actions is unknown. We constructed defined fluorescently labeled trinucleosome arrays, allowing analysis of chromatin conformational dynamics via fluorescence resonance energy transfer (FRET). The arrays undergo reversible Mg^{2+}-dependent folding similar to that of longer arrays studied previously. We define two intermediate conformational states in the reversible folding of the nucleosome arrays and characterize the microscopic rate constants. Nucleosome arrays are highly dynamic even when compact, undergoing conformational fluctuations on timescales in the second to microsecond range. Compact states of the arrays allow binding to DNA within the central nucleosome via site exposure. Protein binding can also drive decompaction of the arrays. Thus, our results reveal multiple modes by which spontaneous chromatin fiber dynamics allow for the invasion and action of DNA-processing protein complexes.

Eukaryotic genomic DNA is wrapped into repeating chains of nucleosomes, which fold into more compact higher-order chromatin structures. DNA that is wrapped in nucleosomes is sterically occluded from large multiprotein assemblies that function on naked DNA substrates, such as RNA and DNA polymerases and repair and recombination enzyme complexes[1]. In addition, both nucleosomal DNA and the linker DNA that connects nucleosomes are further occluded by chromatin folding[2]. Nevertheless, compact heterochromatic DNA undergoes regulated transcription[3,4], repair[5] and recombination[6,7]; gene activator proteins, RNA polymerase and other proteins also readily occupy target sites in heterochromatin[8] and even in highly condensed mitotic chromosomes[9]; and the heterochromatin-associated protein HP1 exchanges rapidly, despite visible compaction of the heterochromatin[10]. How DNA becomes available for crucial genetic functions, when it is wrapped in nucleosomes and further packed into compact chromatin fibers, is not known.

Nucleosomes themselves are highly dynamic, spontaneously undergoing 'site exposure' via conformational fluctuations that make their wrapped DNA transiently accessible to diverse DNA-binding proteins[11,12]. Site exposure provides spontaneous access to the entire nucleosomal DNA length, with particularly rapid and efficient access to the outer-most stretches of the DNA, which spontaneously unwrap as often as once every ~250 ms[13]. Spontaneous site exposure might have a role in photolyase-mediated repair of DNA *in vivo*, which occurs more quickly than can be explained by known ATP-dependent remodeling activities[14]. Such site exposure might also contribute to genome-wide transcriptional regulation *in vivo*[15,16], through a nucleosome-induced cooperativity[17–20].

Could compact chromatin fibers, too, be intrinsically dynamic—compact in the time average, yet spontaneously undergoing transient conformational fluctuations to more accessible states? Such intrinsic dynamics have been postulated[21,22] but have not been demonstrated. Were such compaction and decompaction conformational dynamics to both occur and have suitable rates, they could help to explain how nucleosomes in the middle of long arrays *in vitro* undergo spontaneous site exposure, even when the arrays are highly compact on average[23]. More generally, such dynamics could help to explain how DNA *in vivo* manages to be accessible to the large multiprotein assemblies that carry out many essential genetic processes.

Here we describe studies that reveal rapid spontaneous conformational dynamics in a model reconstituted chromatin fiber, and we show how these conformational dynamics both influence and respond to the binding of a site-specific DNA-binding protein. Our experiments use model nucleosome arrays labeled specifically with fluorescent donor and acceptor dyes, which are placed at particular locations that allow the overall compaction of the arrays or, separately, site exposure within the central nucleosome within the array, to be monitored by FRET[24]. Compact nucleosome arrays prove to be highly dynamic, with significant conformational fluctuations occurring over timescales of microseconds to seconds. There are at least two intermediate conformational states in the reversible unfolding and refolding of the nucleosome arrays; we measure or place bounds on all of the corresponding microscopic rate constants. At least one compact state of the arrays allows binding to DNA inside the central nucleosome via site exposure within that nucleosome. Protein binding can also drive array decompaction.

RESULTS

FRET assay for array compaction and decompaction

We created nucleosome arrays comprising three highly positioned nucleosomes (using our '601' nucleosome-positioning sequence[25]) separated from each other by 20 base pairs (bp) of linker DNA, corresponding to a nucleosome repeat length of 167 bp. Thus, our design exactly reproduces the architecture of the tetranucleosome,

[1]Department of Biochemistry, Molecular Biology and Cell Biology, Northwestern University, Evanston, Illinois, USA. [2]Present address: Department of Physics, The Ohio State University, Columbus, Ohio, USA. Correspondence should be addressed to M.G.P. (mpoirier@mps.ohio-state.edu) or J.W. (j-widom@northwestern.edu).

Received 4 April; accepted 6 July; published online 23 August 2009; doi:10.1038/nsmb.1650

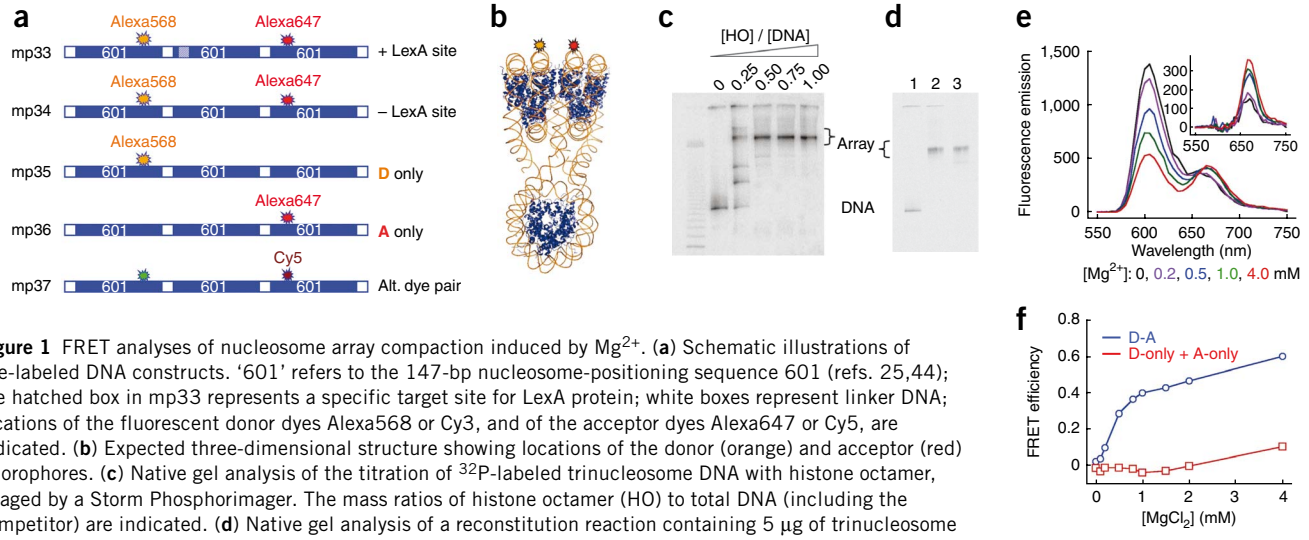

Figure 1 FRET analyses of nucleosome array compaction induced by Mg^{2+}. (**a**) Schematic illustrations of dye-labeled DNA constructs. '601' refers to the 147-bp nucleosome-positioning sequence 601 (refs. 25,44); the hatched box in mp33 represents a specific target site for LexA protein; white boxes represent linker DNA; locations of the fluorescent donor dyes Alexa568 or Cy3, and of the acceptor dyes Alexa647 or Cy5, are indicated. (**b**) Expected three-dimensional structure showing locations of the donor (orange) and acceptor (red) fluorophores. (**c**) Native gel analysis of the titration of ^{32}P-labeled trinucleosome DNA with histone octamer, imaged by a Storm Phosphorimager. The mass ratios of histone octamer (HO) to total DNA (including the competitor) are indicated. (**d**) Native gel analysis of a reconstitution reaction containing 5 μg of trinucleosome DNA, 15 μg of competitor DNA and 15 μg of HO, showing a fluorescence image of the Alexa647 dye. Lane 1, naked DNA; lane 2, after reconstitution; lane 3, after sucrose gradient purification. (**e**) Fluorescence spectra of the FRET-labeled trinucleosomes assembled on DNA mp34 in 0.5× TE buffer plus 0–4.0 mM $MgCl_2$. Inset, spectra after subtracting donor emission. (**f**) Absolute FRET efficiency from data in **e** (blue) and from a parallel titration of a mixture containing 50% donor-only (D-only)- and 50% acceptor-only (A-only)-labeled arrays (red), at the same total array concentration, as a control for aggregation. D-A, donor- and acceptor-labeled arrays.

whose structure is known from X-ray crystallography[26], and the architectures of some of the longer nucleosome oligomers, whose properties have been analyzed in solution and by EM[26–28].

To create a FRET system for analysis of nucleosome array compaction and decompaction, we labeled our trinucleosomes at unique locations on their DNA with fluorescent Alexa568 donor and Alexa647 acceptor dyes (DNA mp34, **Fig. 1a**), such that, if the arrays in solution adopt a compact conformation similar to that observed in the X-ray structure, then the dyes would be close enough together in space to yield efficient FRET (**Fig. 1b**); and, if these arrays undergo conformational changes resulting in significant changes in compactness, the FRET signal would change accordingly. We carried out nucleosome reconstitution onto mp34 DNA and purified the resulting nucleosome arrays on sucrose gradients (**Fig. 1c**,**d**).

In solution, long nucleosome arrays and trinucleosomes are extended (decompacted) in the absence of Mg^{2+} and adopt compact conformations in the presence of increasing concentrations of Mg^{2+} from 0 mM to 1 mM[29] or of NaCl from 5 mM to 100 mM[30]. Titration of our arrays with increasing concentrations of Mg^{2+} was accompanied by a decreasing donor emission (at ~600 nm) and a concomitant increase in the acceptor emission (at ~670 nm) (**Fig. 1e**), implying a substantial increase in FRET efficiency from ~0.0 to ~0.6 (**Fig. 1f**). Several experiments proved that this increase in FRET efficiency arises from a decreased distance between donor and acceptor dyes, implying a Mg^{2+}-dependent compaction of the arrays. These experiments also rule out other possible explanations of the FRET change[24].

The FRET change is not due to dye-specific effects, because arrays labeled at identical locations with Cy3 and Cy5 (DNA mp37) showed similar Mg^{2+}-dependent changes in FRET (data not shown; see below).

Three experiments prove that the FRET increase is not due to aggregation. Titration of an equimolar mixture of arrays labeled with Alexa568 only and with Alexa647 only (DNAs mp35 and mp36, respectively; **Fig. 1a**) showed no FRET increase (**Fig. 1f**). Titration of a different FRET system, in which the donor and acceptor dyes were placed at locations that do not neighbor each other in the compact structure, as defined by X-ray crystallography, did not reveal appreciable compaction in 1 mM Mg^{2+} (DNA mp38; **Supplementary Fig. 1**), but the corresponding mixing experiment did reveal aggregation at higher Mg^{2+} concentration (DNAs mp39 and mp310). Furthermore, measurements of translational diffusion coefficients by fluorescence correlation spectroscopy (FCS) using arrays labeled with donor only (DNA mp35; **Fig. 1a**) showed that the diffusion coefficient of the arrays increased by ~17 ± 2% ($n = 3$) upon addition of 1 mM Mg^{2+}, consistent with increasing compactness and inconsistent with aggregation (**Supplementary Fig. 2**). The 20-bp linker DNAs in these constructs are far shorter than the DNA persistence length in 10 mM Mg^{2+} (~140 bp)[31], so proximity of the donor and acceptor dyes cannot arise from mere flexibility of the linker DNA. Finally, for both dye pairs, most of the FRET change occurred between 0 mM and 1 mM Mg^{2+}, as expected for Mg^{2+}-dependent compaction[29]. Together, these findings show that the trinucleosomes undergo a Mg^{2+}-dependent compaction in solution, as expected. We used this system below to monitor their spontaneous and protein-driven conformational changes.

The characteristic distance (R_0) for 50% FRET efficiency with the Cy3-Cy5 pair is 6 nm[32]. Thus, these FRET values suggest that, in the absence of Mg^{2+}, the arrays are extended, with the dyes on the terminal nucleosomes separated on average by greater than ~10 nm, whereas, in the presence of Mg^{2+}, the arrays are compact, with the dyes separated on average by 5–6 nm[24]. We do not attempt to interpret the FRET changes in terms of exact donor-acceptor distances; however, the apparent ~5–6 nm distance observed in the presence of Mg^{2+} exceeds the ~3–4 nm distance expected on the basis of the crystallographic structure of the tetranucleosome[26]. As will be shown below, this difference is due in part to the compact state being in a rapid dynamic equilibrium with less compact states, such that the time-averaged compactness is less than the greatest possible compactness, which may be observed in the crystal.

FRET assay for site exposure in a nucleosome array

To study how a nucleosome within an array accommodates the binding of an exogenous site-specific DNA-binding protein (we chose for convenience the *Escherichia coli* repressor protein LexA), we designed a second FRET-labeled array system (**Fig. 2a**,**b**) in which both dyes are placed on the central nucleosome at locations such that the resulting

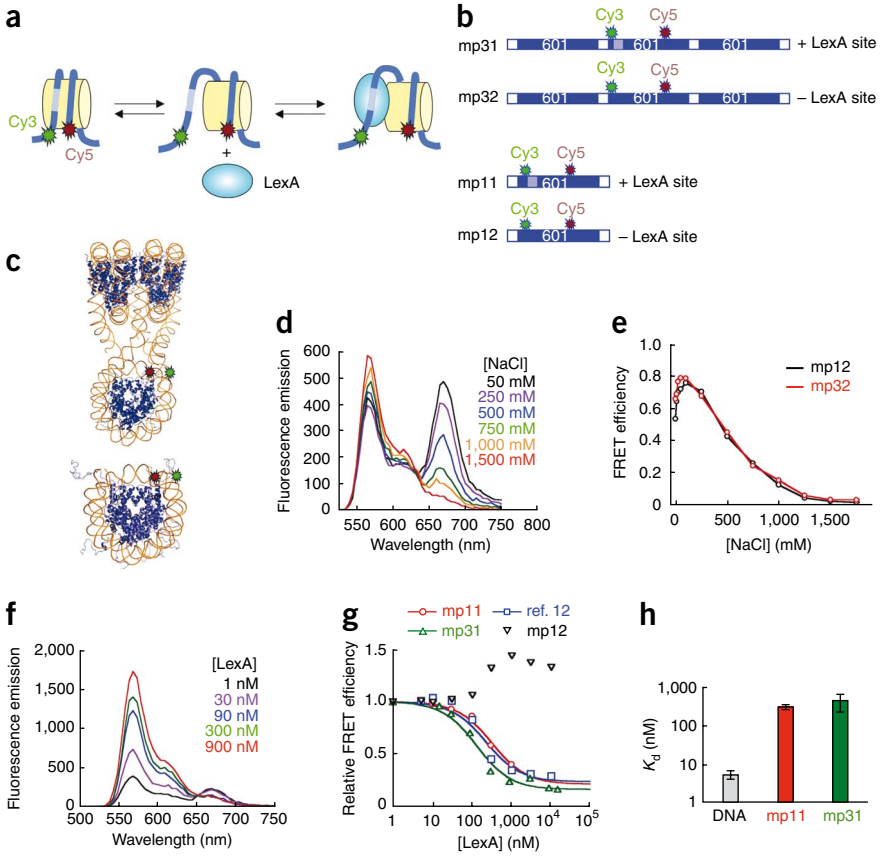

Figure 2 FRET analyses of site exposure in mononucleosomes and in nucleosome arrays in the absence of Mg^{2+}. (**a**) Schematic illustration of FRET system for detecting site exposure. A mononucleosome system is shown. The approximate locations of Cy3 donor and Cy5 acceptor dyes are indicated. Site exposure occurs via unwrapping from a DNA end[12], increasing the distance between donor and acceptor and thus decreasing the FRET, while freeing up the LexA target site (hatched). Binding of LexA traps the nucleosome in this open state. (**b**) Schematic illustrations of dye-labeled DNA constructs. (**c**) Expected three-dimensional structure showing locations of the donor (green) and acceptor (red) fluorophores. (**d**) Fluorescence spectra of mp32 trinucleosome arrays titrated with NaCl from 0–1.5 M. (**e**) Absolute FRET efficiencies from the data in **d** and from a parallel titration on mononucleosomes (black). (**f**) Fluorescence spectra of mp31 trinucleosome arrays titrated with LexA protein from 1 nM to 900 nM. (**g**) Quantitative FRET analysis of LexA titrations from **e** together with parallel titrations on mononucleosome systems with (mp11) or without (mp12) LexA target sites, also showing results obtained on a related LexA site-containing mononucleosome system having the acceptor dye on the histone core (residue 35 of histone H3)[12] instead of on the DNA. Curves are fits to simple binding isotherms[12]. (**h**) Apparent binding affinities (dissociation constants) of LexA from measurements such as those in **f** obtained by fitting the FRET data to a simple binding isotherm. Error bars indicate s.d. ($n = 2$).

FRET signal is sensitive to site-exposure conformational changes in this nucleosome (shown schematically in **Fig. 2a** for the case of a mononucleosome; see also refs. 12,13). When the DNA of this labeled nucleosome is in the fully wrapped state, a high FRET signal will be observed. Site exposure increases the distance between donor and acceptor, decreasing the FRET and freeing up the LexA-binding site. Binding of LexA protein to the exposed target site traps the nucleosome in this site-exposed low-FRET state.

We created variants of this FRET-labeled nucleosome array with and without a binding site for LexA protein inside the labeled nucleosome (DNAs mp31 and mp32; **Fig. 2b**) at the identical location within this nucleosome to that analyzed previously[12,13]. FRET changes that we might observe could be due to changes in nucleosome packing within the array, rather than to conformational changes within the central nucleosome itself. To control for this possibility, we created FRET-labeled mononucleosomes identical to the labeled central nucleosome of the array (with or without a LexA site) using DNAs mp11 and mp12 (**Fig. 2b**,**c**). Nucleosomes were reconstituted onto FRET-labeled array or mononucleosome DNA and the resulting reconstituted products further purified (**Supplementary Fig. 3**).

Two titration experiments confirmed that these FRET systems properly monitor site exposure-conformational changes within the central nucleosome of the array: first, using NaCl, which destabilizes the wrapping of the nucleosomal DNA (and, at sufficiently high concentrations, drives the histones off altogether)[12,13]; and second, using LexA protein, which binds to its nucleosomal DNA target site only when that nucleosome undergoes a site-exposure conformational change[12,13].

Titration of these arrays with NaCl (**Fig. 2d**) leads to increasing Cy3 emission and decreasing Cy5 emission, implying a substantial decrease in FRET (**Fig. 2e**), as expected for a system monitoring the unwrapping of DNA in the central nucleosome. The decreasing FRET arises from the progressively increasing fraction of time that the DNA in the labeled nucleosome spends partially (or, at high NaCl concentrations, completely) unwrapped off the histone surface[12,13,33]. Similar titrations on mononucleosomes gave identical results (**Fig. 2e**). These results confirm that the FRET changes observed with the arrays are not due to changes in packing of nucleosomes within the array but, instead, reflect conformational changes within the labeled central nucleosome.

Titration of these arrays with LexA protein (here done in the absence of Mg^{2+}, so that the arrays are extended) also led to a decrease in FRET (**Fig. 2f**,**g**). Thus, as expected, LexA binds to the central nucleosome within the array, and binding is coupled to partial unwrapping (site exposure) of the DNA of this nucleosome. The DNA unwrapping is only partial, because the FRET does not decrease to zero, even at near-saturating LexA concentrations. This FRET system is sensitive only to site-specific binding of LexA, not to nonspecific binding, because titration of a FRET-labeled nucleosome lacking a specific LexA target site did not decrease the FRET (**Fig. 2g**). We obtained quantitatively identical results for specific binding by LexA with the mononucleosome and array systems (**Fig. 2g**,**h**). Thus, site exposure in the central nucleosome of extended arrays is negligibly influenced by the existence of neighboring nucleosomes.

Binding via site exposure in a compact array

The above data show that we have established two different kinds of FRET system: one that monitors overall compaction of the array (**Fig. 1**); and one that monitors site-exposure conformational changes within the central nucleosome (**Fig. 2**). We used these systems to ask

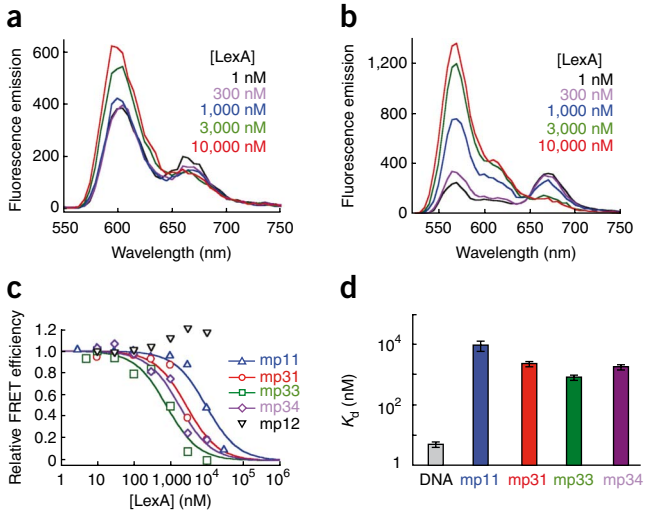

Figure 3 FRET analyses of site exposure and decompaction for nucleosome arrays in 1 mM Mg^{2+}. (**a**) LexA titration of compaction-sensitive nucleosome arrays (DNA mp33) in 1 mM Mg^{2+}, monitored by FRET. (**b**) As in **a**, except using site exposure–sensitive arrays (DNA mp31). (**c**) Quantitative analysis of titrations from **a**,**b** and additional systems: compaction-sensitive arrays lacking a LexA site (mp34), and site exposure–sensitive mononucleosomes having (mp11) or lacking (mp12) a LexA site. (**d**) Apparent binding affinities (dissociation constants) of LexA from measurements such as those in **c**. Error bars indicate s.d. (n = 2–3).

whether LexA binding couples to changes in the conformation of nucleosome arrays when the arrays start out in their compact state. Our previous work[23] allowed us to ask how array compaction influenced protein binding but did not allow analysis of what happens to the array when the proteins bind. Our new FRET systems provide both kinds of information directly.

We titrated FRET-labeled arrays that are sensitive to array compactness (mp33) or to site exposure in the central nucleosome (mp31) with increasing concentrations of LexA protein in solutions containing 1 mM Mg^{2+}, such that, before addition of LexA, the arrays are compact. As expected, in zero or very low LexA concentrations, the compactness-sensitive arrays showed high FRET (**Fig. 3a**), showing that they are indeed compact. Correspondingly, under the same conditions, the site exposure–sensitive arrays showed high FRET (**Fig. 3b**), indicating that the central nucleosome's DNA is fully wrapped. Increasing concentrations of LexA lead to decreasing FRET in both systems (**Fig. 3a**,**b**).

Consistent with our analysis of restriction enzyme accessibility in nucleosome 17-mer arrays[23], quantitative analysis of the data from the site exposure–sensitive arrays (**Fig. 3c**,**d**) showed that LexA binds to its target site in the middle of the compact array with no reduction in affinity (if anything, a slight increase in affinity) compared to binding to the same site in a mononucleosome (compare DNA mp31 with mp11). Binding was accompanied by loss of the intranucleosomal FRET signal, but only if the nucleosome contained a specific LexA target site (compare DNA mp11 with mp12). Thus, these data establish that proteins can bind site specifically to target sites inside a nucleosome in the middle of a compact nucleosome array and, for the first time, show that this binding occurs via site exposure within the central nucleosome.

Array decompaction driven by nonspecific LexA binding

To assess whether LexA binding influenced the overall compaction of the arrays, we carried out LexA titrations parallel to those described above, except using the compaction-sensitive FRET system. Binding of LexA is accompanied by decompaction of the arrays (**Fig. 3c**,**d**). Notably, however, equivalent results were obtained regardless of whether the arrays contained a specific LexA-binding site within the central nucleosome or not (compare DNA mp33 with mp34). Thus, whereas the site-exposed state is driven to high occupancy only by site-specific LexA binding, decompaction of the arrays is driven by nonspecific LexA binding. We presume that the relevant nonspecific binding is to the linker DNA (see Discussion); indeed, as we shall discuss there, this outcome is predicted from our analyses of restriction enzyme accessibility within nucleosome 17-mer arrays[23].

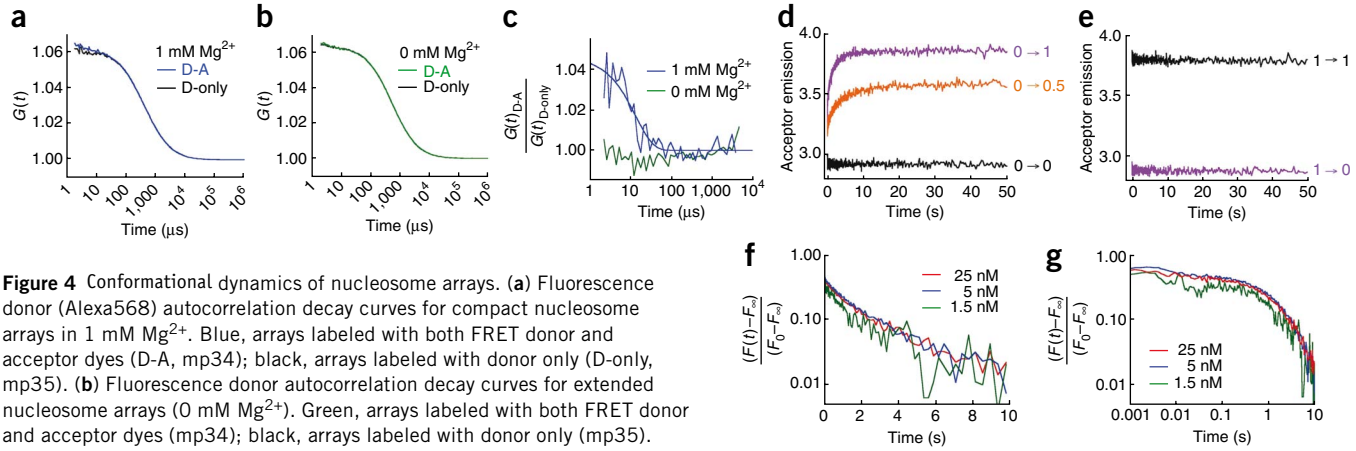

Figure 4 Conformational dynamics of nucleosome arrays. (**a**) Fluorescence donor (Alexa568) autocorrelation decay curves for compact nucleosome arrays in 1 mM Mg^{2+}. Blue, arrays labeled with both FRET donor and acceptor dyes (D-A, mp34); black, arrays labeled with donor only (D-only, mp35). (**b**) Fluorescence donor autocorrelation decay curves for extended nucleosome arrays (0 mM Mg^{2+}). Green, arrays labeled with both FRET donor and acceptor dyes (mp34); black, arrays labeled with donor only (mp35). (**c**) Ratios of donor autocorrelation decay in presence of acceptor to decay with donor-only, from the data of **a** (blue) and **b** (green). (**d**) Stopped-flow FRET analysis of kinetics of nucleosome array compaction. Equal volumes of compaction-sensitive nucleosome arrays (DNA mp37) that were in their extended state (0 mM Mg^{2+}) were rapidly mixed with $MgCl_2$, and Cy5 emission was monitored. The final concentration of the arrays was 5 nM; final concentrations of $MgCl_2$ are indicated. (**e**) Stopped-flow FRET analysis of array decompaction. As in **d**, except the arrays were initially compact in 1 mM Mg^{2+} and then they were rapidly mixed with an excess of EDTA (final concentration 2 mM), so that the effective final Mg^{2+} concentration is zero. (**f**) Quantitative analysis of array compaction kinetics, for 1 mM Mg^{2+} (final) and final concentrations of arrays of 1.5, 5 and 25 nM (indicated). $F(t)$, measured Cy5 fluorescence at time (t); F_0, intensity at time 0; $F\infty$, fluorescence at long timescales. (**g**) As in **f**, except plotted with time on a log scale.

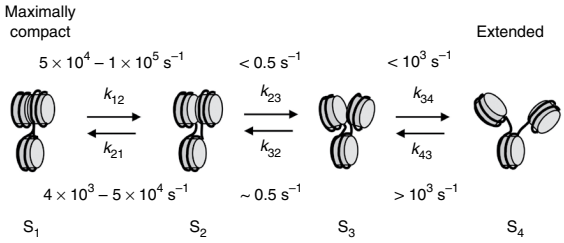

Figure 5 Minimal kinetic scheme for nucleosome array dynamics in 1 mM Mg^{2+}. The stopped-flow FRET experiments (**Fig. 4d,f,g**) show compaction kinetics, requiring a minimum of three conformational states, with the second forward step ($S_3 \rightarrow S_2$, rate k_{32}) and reverse step ($S_2 \rightarrow S_3$, rate k_{23}) being slower than the first forward step ($S_4 \rightarrow S_3$, rate k_{43}). The equilibrium titrations (**Fig. 1**) demonstrate that the arrays are compact (in the time average) in 1 mM Mg^{2+}, but the FRET-FCS experiment (**Fig. 4a,c**) demonstrates rapid interconversion between two states, with a relaxation time of ~10^{-5} s, much faster than the rates for $S_3 \leftrightarrow S_2$, therefore requiring at least one additional compact state (S_1) connected reversibly to S_2. The corresponding rates (or the bounds on them) imply that only states S_1 and S_2 are significantly populated in 1 mM Mg^{2+}; however, the central nucleosomes of compact arrays undergo nucleosomal site exposure and bind LexA protein, just as for mononucleosomes. Thus, states S_1 and/or S_2 are competent for nucleosomal site exposure. See **Supplementary Discussion** for further details of the kinetic analysis. The structures shown are intended only to represent that compactness increases progressively (decreasing distance from nucleosome 1 to nucleosome 3) as the arrays evolve from state S_4 to S_1.

Dynamics of array compaction and decompaction

How is it that DNA-binding proteins can bind via site exposure to a nucleosome inside a compact array? The simplest possibility is that perhaps the compact state of the arrays is not a frozen, inert conformational state, as imaged by X-ray crystallography[26], but instead might be dynamic, fluctuating between more and less compact conformations in some manner that makes site exposure possible. This idea is analogous to how we currently understand the binding of proteins to target sites inside isolated nucleosomes to occur: binding occurs via intrinsic nucleosome conformational dynamics (site exposure), which happens spontaneously and with high frequency, preceding and allowing the subsequent binding of a protein to a now freely accessible nucleosomal DNA target site[13].

If this reasoning is correct, it follows that nucleosome arrays should show rapid transient conformational fluctuations between decompacted and recompacted states, even in the absence of any other exogenous DNA-binding proteins, and even in solution conditions (such as 1 mM Mg^{2+}) in which the arrays are compact in the time average. If compaction and decompaction fluctuations were limited by diffusion, they might occur rapidly, because nucleosomes diffuse a distance comparable to their diameter in just microseconds[34]. However, if a large energy barrier separates the compact and decompacted states, the actual timescale could be far slower.

As there is at present no information even on the existence of such potential nucleosome array conformational dynamics, let alone on their timescales, we took two complementary approaches that together span the entire relevant range of timescales. FRET-FCS allows the analysis of conformational fluctuations on timescales of microseconds to tens of milliseconds, whereas stopped-flow FRET allows analyses for timescales of milliseconds or longer. Both experiments are sensitive only to conformational changes that are large enough to yield significant changes in FRET.

The FRET-FCS experiment measures the ratio of fluorescence donor intensity autocorrelation functions for nucleosome arrays labeled with both donor and acceptor (DNA mp34) and, separately, for arrays labeled with donor only (DNA mp35), thereby eliminating contributions from diffusion. If nucleosome arrays undergo reversible interconversion between two conformational states, one more compact (high FRET) and one less compact (low FRET), and if these fluctuations occur within microseconds to tens of milliseconds, this will be manifested as an exponentially decaying ratio function with a characteristic decay time equal to the sum of the decompaction plus recompaction rate constants[13].

Indeed, FRET-FCS analysis (**Fig. 4**) revealed an exponentially decaying ratio autocorrelation function with a decay time of ~10^{-5} s, implying that nucleosome arrays that, on average, are compacted (in 1 mM Mg^{2+}) undergo spontaneous rapid but transient fluctuations to less compact conformations and back, remarkably quickly: ~10^5 times per second. The small amplitude of the ratio function (**Fig. 4c**) implies either that the two states are roughly equally populated but that the more compact state is only slightly more compact (slightly greater FRET) or, alternatively, that the more compact state is substantially more compact (substantially greater FRET) but is populated only with low probability. As expected, no decay is observed for arrays in the absence of Mg^{2+}, where compact states have negligible probability.

Our stopped-flow FRET experiments started with extended nucleosome arrays (in 0 mM Mg^{2+}); we then rapidly added 1 mM Mg^{2+} and measured the rate at which the arrays compact, as monitored by the corresponding increase in FRET. The resulting data revealed a large instantaneous increase in FRET, together with a slower (but still rapid), further FRET increase of comparable magnitude (**Fig. 4d**). The instantaneous FRET increase implies a corresponding increase in array compactness that occurs faster than the mixing dead time of the stopped-flow instrument, which is ~10^{-3} s, whereas the subsequent FRET increase, having a time constant of ~2 s, implies a subsequent further increase in array compactness. Both the instantaneous and slower phases of these kinetics reflect intramolecular conformational changes, not aggregation and disaggregation, because both rate constants are independent of array concentration over a 17-fold range (**Fig. 4f,g**).

Stopped-flow FRET also allows us to investigate the kinetics of decompaction. We start with compact arrays (in 1 mM Mg^{2+}), then rapidly add excess EDTA, chelating the Mg^{2+}, such that the stable conformation of the arrays is now the extended state. Decompaction of the arrays is monitored by the corresponding loss of FRET. (Note that this experiment measures decompaction in 0 mM Mg^{2+}.) In these experiments, the decompaction reached completion within the mixing dead time (~10^{-3} s; **Fig. 4e**).

The simplest kinetic mechanism that integrates the equilibrium and kinetic data for 1 mM Mg^{2+} (**Figs. 1** and **4**, respectively) requires a minimum of four conformational states (that is, states with differing FRET efficiencies) (**Fig. 5** and **Supplementary Discussion**), with at least two conformational intermediates between the most compact and the most extended states of the arrays.

DISCUSSION

Model system for analysis of nucleosome array dynamics

Our array system exactly reproduces the architecture of three consecutive nucleosomes that adopt a compact structure in the tetranucleosomes investigated by X-ray crystallography[26], as well as of 12-mer nucleosome arrays analyzed in solution and by EM[26–29]. Consistent with expectations from those studies and from another study of trinucleosomes[30], our arrays show a reversible Mg^{2+}

concentration–dependent compaction (**Fig. 1**). Moreover, the ability of proteins to bind site-specifically to target sites inside the central nucleosome of our trinucleosomes (**Fig. 2**) agrees quantitatively with our results on binding inside the central nucleosome in a closely similar 17-mer nucleosome array[23]. Thus, although highly simplified, our trinucleosomes capture essential aspects of the behavior of the tetramer and longer nucleosome arrays, which are widely used as model systems for studies of chromatin structure and function[23,26,27,29,35,36]. As in many of these other studies, our system lacks the 'linker histone' H1, which influences chromatin structure and accessibility[30,37]. Omission of H1 is justified by the findings that H1 is not essential for viability in some eukaryotes[38] and is not a stoichiometric structural component of chromatin[39,40].

Site exposure in compact nucleosome arrays

In our earlier studies on mononucleosomes, we proposed[11] and later proved[12,13,41] that site-specific DNA-binding proteins can bind to target sites that (in the time average) are buried inside nucleosomes and that the mechanism of this binding is via spontaneous partial unwrapping (site exposure) of the nucleosomal DNA. The rate of unwrapping that is sufficient to expose a LexA site at the same location as in this present study is 4 s^{-1} (DNA remains fully wrapped for only ~250 ms before spontaneously unwrapping), and the rewrapping rate is 20–90 s^{-1} (once unwrapped, DNA rewraps after just 10–50 ms). Note that the actual rate of binding depends on a protein's concentration. At low concentrations—for example, in restriction enzyme assays—site exposure occurs in a rapid pre-equilibrium regime, with rewrapping competing kinetically with protein binding[11,41–43]. However, at high concentrations, easily reached *in vitro*, the binding rate exceeds the rewrapping rate, and unwrapping becomes rate limiting[13]. Our subsequent studies showed that buried nucleosomal DNA target sites remain similarly accessible to restriction enzymes, even when those nucleosomes are present in long arrays and even when these arrays are (in the time average) highly compact[23]. Thus, it was natural to imagine that binding of proteins to target sites inside nucleosomes in long nucleosome arrays might also be made possible by spontaneous site exposure, but whether and how site exposure could actually occur inside highly compact arrays was not known. Appropriate conformational dynamics within the arrays could certainly help, but whether such dynamics actually occur was not known either.

Our new results answer these questions. Nucleosome arrays are compact in 1 mM Mg^{2+} (**Figs. 1** and **4** and **Supplementary Figs. 1** and **2**), driven nearly completely into a pair of compact states, S_1 and S_2 (**Fig. 5**). Moreover, these compact states are highly dynamic, interconverting on an exceptionally fast timescale of ~10 μs. Substantial FRET fluctuations imply substantial changes in distance. Note, however, that the existence of a populated but less-than-maximally compact state in 1 mM Mg^{2+} (S_2) could also cause the steady-state FRET (**Fig. 1**) to be lower than expected on the basis of the X-ray structure. Not only are the compact nucleosome arrays highly dynamic, they are dynamic in a way that allows for binding of the LexA protein via site exposure within the central nucleosome of the compact arrays (**Fig. 3**). DNA unwrapping (the hallmark of site exposure) is demonstrated by the accompanying LexA-dependent decrease in intranucleosomal FRET, which implies that the end segment of nucleosomal DNA (where the donor is attached) moves away from the middle stretch of that same nucleosome's DNA (where the acceptor is attached) coupled to LexA binding. Finally, for both compact and extended arrays, the quantitative extents of binding via site exposure were similar for the arrays compared to mononucleosomes (**Figs. 2** and **3**), as we found previously with longer arrays[23].

Protein binding can drive decompaction of nucleosome arrays

Binding of LexA protein to its target site within the central nucleosome is accompanied by decompaction of the array (**Fig. 3c**). However, this decompaction is not attributable to the site-exposure conformational change, because, when nucleosomes lack a LexA target site, addition of LexA protein does not drive formation of the site-exposed state[12,13] (**Fig. 2g**). Still, the arrays nevertheless decompact (**Fig. 3c**). It follows that array decompaction is driven by nonspecific LexA binding. Moreover, the concentrations of LexA required to induce array decompaction exceed the dissociation constant for nonspecific binding of LexA to naked DNA (~300 nM)[12], so nonspecific binding is expected.

This nonspecific LexA binding is most likely to occur to linker DNA, because linker DNA more closely resembles ordinary B-form DNA than does nucleosomal DNA[26] (and thus is more-recognizable by LexA) and because linker DNA is much more accessible than is wrapped nucleosomal DNA[23]. Moreover, we expect on thermodynamic grounds that binding of proteins to linker DNA should cause array decompaction: our studies on 17-mer nucleosome arrays[23] showed that array compaction strongly reduced binding to linker DNA compared to binding to naked DNA. As chromatin compaction destabilizes protein binding to linker DNA, it follows from thermodynamic linkage that the opposite should equally be true: binding to linker DNA should destabilize the compact state of the nucleosome array, driving array decompaction.

Indeed, both of these effects are simultaneously manifested in the present study. We see a large reduction in LexA binding affinity for nonspecific binding to the compact array (~1,800 nM for half-maximal effect for the arrays lacking a specific LexA site, versus ~300 nM for nonspecific binding to naked DNA); at the same time, when binding is driven by sufficiently high LexA concentrations, it is accompanied by decompaction of the array.

In summary, our results demonstrate that protein binding to nucleosome arrays, most likely to the linker DNA, can cause complete decompaction of the arrays. This decompaction could in principle be regulated and have important consequences for the binding of other proteins to chromatin and, ultimately, for biological function.

METHODS

Methods and any associated references are available in the online version of the paper at http://www.nature.com/nsmb/.

Note: Supplementary information is available on the Nature Structural & Molecular Biology website.

ACKNOWLEDGMENTS

We thank E. Elson (Washington University) and E. Matayoshi (Abbott Laboratories) for access to Zeiss Confocor 2 instruments, on which preliminary FCS experiments were carried out. We thank J. Little (University of Arizona) for the LexA expression plasmid. We thank E. Elson and E. Matayoshi and members of the Widom laboratory for discussions, K. Swinger (Northwestern University) for help with the trinucleosome structure figures and the Keck Biophysics and Biological Imaging Facilities at Northwestern University for the use of instruments. M.G.P. acknowledges support from US National Institutes of Health postdoctoral fellowship F32 GM072306 and a Career Award in the Biomedical Sciences from the Burroughs-Wellcome Fund. J.W. acknowledges research support from US National Institutes of Health grants R01 GM54692 and R01 GM58617.

AUTHOR CONTRIBUTIONS

M.G.P. designed, executed and interpreted experiments and wrote some of the paper; E.O. designed, executed and interpreted experiments; H.S.T. designed, executed and interpreted experiments; J.W. designed and interpreted experiments and wrote some of the paper.

Published online at http://www.nature.com/nsmb/.
Reprints and permissions information is available online at http://npg.nature.com/reprintsandpermissions/.

1. Richmond, T.J. & Davey, C. The structure of DNA in the nucleosome core. *Nature* **423**, 145–150 (2003).
2. Robinson, P.J. & Rhodes, D. Structure of the '30 nm' chromatin fibre: a key role for the linker histone. *Curr. Opin. Struct. Biol.* **16**, 336–343 (2006).
3. Grewal, S.I. & Elgin, S.C. Transcription and RNA interference in the formation of heterochromatin. *Nature* **447**, 399–406 (2007).
4. Bühler, M. & Moazed, D. Transcription and RNAi in heterochromatic gene silencing. *Nat. Struct. Mol. Biol.* **14**, 1041–1048 (2007).
5. Fousteri, M., van Hoffen, A., Vargova, H. & Mullenders, L.H. Repair of DNA lesions in chromosomal DNA impact of chromatin structure and Cockayne syndrome proteins. *DNA Repair (Amst.)* **4**, 919–925 (2005).
6. Topp, C.N. & Dawe, R.K. Reinterpreting pericentromeric heterochromatin. *Curr. Opin. Plant Biol.* **9**, 647–653 (2006).
7. Brutlag, D.L. Molecular arrangement and evolution of heterochromatic DNA. *Annu. Rev. Genet.* **14**, 121–144 (1980).
8. Chen, L. & Widom, J. Mechanism of transcriptional silencing in yeast. *Cell* **120**, 37–48 (2005).
9. Chen, D. *et al.* Condensed mitotic chromatin is accessible to transcription factors and chromatin structural proteins. *J. Cell Biol.* **168**, 41–54 (2005).
10. Cheutin, T. *et al.* Maintenance of stable heterochromatin domains by dynamic HP1 binding. *Science* **299**, 721–725 (2003).
11. Polach, K.J. & Widom, J. Mechanism of protein access to specific DNA sequences in chromatin: a dynamic equilibrium model for gene regulation. *J. Mol. Biol.* **254**, 130–149 (1995).
12. Li, G. & Widom, J. Nucleosomes facilitate their own invasion. *Nat. Struct. Mol. Biol.* **11**, 763–769 (2004).
13. Li, G., Levitus, M., Bustamante, C. & Widom, J. Rapid spontaneous accessibility of nucleosomal DNA. *Nat. Struct. Mol. Biol.* **12**, 46–53 (2005).
14. Bucceri, A., Kapitza, K. & Thoma, F. Rapid accessibility of nucleosomal DNA in yeast on a second time scale. *EMBO J.* **25**, 3123–3132 (2006).
15. Bernstein, B.E., Liu, C., Humphrey, E.L., Perlstein, E.O. & Schreiber, S. Global nucleosome occupancy in yeast. *Genome Biol.* **5**, R62 (2004).
16. Tirosh, I. & Barkai, N. Two strategies for gene regulation by promoter nucleosomes. *Genome Res.* **18**, 1084–1091 (2008).
17. Adams, C.C. & Workman, J.L. Binding of disparate transcriptional activators to nucleosomal DNA is inherently cooperative. *Mol. Cell. Biol.* **15**, 1405–1421 (1995).
18. Polach, K.J. & Widom, J. A model for the cooperative binding of eukaryotic regulatory proteins to nucleosomal target sites. *J. Mol. Biol.* **258**, 800–812 (1996).
19. Miller, J.A. & Widom, J. Collaborative competition mechanism for gene activation *in vivo*. *Mol. Cell. Biol.* **23**, 1623–1632 (2003.).
20. Vashee, S., Willie, J. & Kodadek, T. Synergistic activation of transcription by physiologically unrelated transcription factors through cooperative DNA-binding. *Biochem. Biophys. Res. Commun.* **247**, 530–535 (1998).
21. Luger, K. & Hansen, J.C. Nucleosome and chromatin fiber dynamics. *Curr. Opin. Struct. Biol.* **15**, 188–196 (2005).
22. Widom, J. Toward a unified model of chromatin folding. *Annu. Rev. Biophys. Biophys. Chem.* **18**, 365–395 (1989).
23. Poirier, M.G., Bussiek, M., Langowski, J. & Widom, J. Spontaneous access to DNA target sites in folded chromatin fibers. *J. Mol. Biol.* **379**, 772–786 (2008).
24. Clegg, R.M. Fluorescence resonance energy transfer and nucleic acids. *Methods Enzymol.* **211**, 353–388 (1992).
25. Lowary, P.T. & Widom, J. New DNA sequence rules for high affinity binding to histone octamer and sequence-directed nucleosome positioning. *J. Mol. Biol.* **276**, 19–42 (1998).
26. Schalch, T., Duda, S., Sargent, D. & Richmond, T. X-ray structure of a tetranucleosome and its implications for the chromatin fibre. *Nature* **436**, 138–141 (2005).
27. Dorigo, B. *et al.* Nucleosome arrays reveal the two-start organization of the chromatin fiber. *Science* **306**, 1571–1573 (2004).
28. Routh, A., Sandin, S. & Rhodes, D. Nucleosome repeat length and linker histone stoichiometry determine chromatin fiber structure. *Proc. Natl. Acad. Sci. USA* **105**, 8872–8877 (2008).
29. Dorigo, B., Schalch, T., Bystricky, K. & Richmond, T. Chromatin fiber folding: requirement for the histone H4 N-terminal tail. *J. Mol. Biol.* **327**, 85–96 (2003).
30. Bussiek, M., Tóth, K., Schwarz, N. & Langowski, J. Trinucleosome compaction studied by fluorescence energy transfer and scanning force microscopy. *Biochemistry* **45**, 10838–10846 (2006).
31. Du, Q., Smith, C., Shiffeldrim, N., Vologodskaia, M. & Vologodskii, A. Cyclization of short DNA fragments and bending fluctuations of the double helix. *Proc. Natl. Acad. Sci. USA* **102**, 5397–5402 (2005).
32. Iqbal, A. *et al.* Orientation dependence in fluorescent energy transfer between Cy3 and Cy5 terminally attached to double-stranded nucleic acids. *Proc. Natl. Acad. Sci. USA* **105**, 11176–11181 (2008).
33. Bao, Y., White, C.L. & Luger, K. Nucleosome core particles containing a poly(dA. dT) sequence element exhibit a locally distorted DNA structure. *J. Mol. Biol.* **361**, 617–624 (2006).
34. Yao, J., Lowary, P.T. & Widom, J. Direct detection of linker DNA bending in defined-length oligomers of chromatin. *Proc. Natl. Acad. Sci. USA* **87**, 7603–7607 (1990).
35. Robinson, P.J., Fairall, L., Huynh, V.A. & Rhodes, D. EM measurements define the dimensions of the '30-nm' chromatin fiber: evidence for a compact, interdigitated structure. *Proc. Natl. Acad. Sci. USA* **103**, 6506–6511 (2006).
36. Shogren-Knaak, M. *et al.* Histone H4–K16 acetylation controls chromatin structure and protein interactions. *Science* **311**, 844–847 (2006).
37. Widom, J. Chromatin structure: linking structure to function with histone H1. *Curr. Biol.* **8**, R788–R791 (1998).
38. Ushinsky, S.C. *et al.* Histone H1 in *Saccharomyces cerevisiae*. *Yeast* **13**, 151–161 (1997).
39. Bates, D.L. & Thomas, J.O. Histones H1 and H5: one or two molecules per nucleosome? *Nucleic Acids Res.* **9**, 5883–5894 (1981).
40. Fan, Y. *et al.* Histone H1 depletion in mammals alters global chromatin structure but causes specific changes in gene regulation. *Cell* **123**, 1199–1212 (2005).
41. Anderson, J.D., Thåström, A. & Widom, J. Spontaneous access of proteins to buried nucleosomal DNA target sites occurs via a mechanism that is distinct from nucleosome translocation. *Mol. Cell. Biol.* **22**, 7147–7157 (2002).
42. Anderson, J.D. & Widom, J. Sequence and position-dependence of the equilibrium accessibility of nucleosomal DNA target sites. *J. Mol. Biol.* **296**, 979–987 (2000).
43. Polach, K.J. & Widom, J. Restriction enzymes as probes of nucleosome stability and dynamics. *Methods Enzymol.* **304**, 278–298 (1999).
44. Thåström, A., Bingham, L.M. & Widom, J. Nucleosomal locations of dominant DNA sequence motifs for histone-DNA interactions and nucleosome positioning. *J. Mol. Biol.* **338**, 695–709 (2004).

ONLINE METHODS

Labeling DNA oligonucleotides. We incorporated amine-reactive Alexa568 and Alexa647 (Invitrogen), or Cy3 and Cy5 (Amersham), into amino-dT–containing oligos by PCR with labeled DNA oligos. Oligos were ethanol precipitated, washed and resuspended in NaH_2BO_3, pH8.5. We dissolved the reactive dye in DMSO, added it to the oligos in a five-fold molar excess and incubated the mixture at room temperature (21–22 °C) overnight. The labeled oligos were ethanol precipitated twice, then purified by reverse-phase HPLC on a C18 column with an acetonitrille gradient. The gradient resolved free dye, unlabeled oligos and the desired dye-labeled oligos.

Preparation of labeled double-stranded DNA. See **Supplementary Methods** for details. We used PCR to prepare labeled mononucleosome DNA and each nucleosome DNA of the trinucleosome templates. We used fluorophore-labeled DNA oligos to incorporate Cy3 at base pair 3 and Cy5 at the base pair 83 in the 147-bp nucleosome-positioning sequence (NPS) of DNAs mp11 and mp12, and within the central NPS of DNAs mp31 and mp32. Some sequences contained the 20-bp binding site of LexA between base pairs 8–27 of the NPS. Fluorophore-labeled DNA oligos were also used to incorporate Cy3 or Alexa568 at base pair 112 of the left-hand NPS and/or Cy5 or Alexa647 at base pair 35 of the right-hand NPS (DNAs mp31–37). Two different asymmetric TspRI sites were incorporated outside each NPS sequence. Each NPS sequence was digested by TspRI and phenol-chloroform extracted. The three NPSs were combined at equal molar ratios, ligated, phenol-chloroform extracted and purified by PAGE.

Proteins. We purified histone octamer from chicken erythrocytes as described[45]. We expressed LexA from plasmid pJWL228 (gift from J. Little) and purified it as described[46].

Nucleosome array reconstitutions. We reconstituted mononucleosomes by double dialysis from 0.5× TE, 2 M NaCl, 1 mM benzamidine hydrochloride (BZA), 5 µg of 601 DNA, 15 µg of long salmon sperm DNA (10–50 kb), 10 µg of histone octamer and trace amounts of ^{32}P-labeled 601 DNA[47] in a total volume of 50 µl. We then purified the nucleosomes away from the salmon sperm DNA and any aggregates on sucrose gradients[25] and assayed them by native 5% PAGE, visualizing themusing a Phosphorimager (^{32}P) or fluorimager (Cy5, Alexa647). We reconstituted trinucleosomes as described above, except using 5 µg of 601 trimer DNA, 15 µg core particle DNA, 15 µg histone octamer and trace amounts of ^{32}P-labeled trimer DNA. We then purified them on sucrose gradients and assayed them by native 4% PAGE.

LexA binding. We estimated the binding affinity of LexA to the DNA constructs by electrophoretic mobility shift assay (EMSA). We incubated radiolabeled DNA at 0.1 nM with LexA for 5 min in 0.5× TE or 5mM Tris + 1mM $MgCl_2$. Ficoll was added to 3% (w/v) and the samples analyzed by native 5% PAGE run in 1/3× TBE or 1/3× TB + 1mM $MgCl_2$, then analyzed by Phosphorimager.

Fluorescence measurements. We used an ISS PC1 photon-counting spectrometer to acquire fluorescence spectra, with additional 550-nm or 570-nm cut-on filters for Cy3/Cy5 or Alexa568/Alexa647 arrays, respectively, in the emission channel. Cy3 was excited at 515 nm; Cy5 was directly excited at 610 nm. Alexa568 was excited at 545 nm; Alexa647 was directly excited at 625 nm. All $MgCl_2$ and LexA titrations were carried out with 2 nM trinucleosomes or 6 nM mononucleosomes.

Fret efficiency measurements. We used the $(\text{ratio})_A$ method[24] to determine the FRET efficiency, E:

$$E = \frac{\left(\varepsilon^A(\lambda'')\frac{F^A(\lambda')}{F^A(\lambda'')} - \varepsilon^A(\lambda')\right)}{\varepsilon^D(\lambda')d^+} \quad (1)$$

$F^A(\lambda)$ is the fluorescence emission of the acceptor (Cy5, Alexa647), when excited by the wavelength, λ. $\varepsilon^D(\lambda)$ and $\varepsilon^A(\lambda)$ are extinction coefficients of the donor (Cy3, Alexa568) and acceptor (Cy5, Alexa647), at λ. d^+ is the fraction of molecules labeled with acceptor; λ′ is the wavelength for donor excitation; λ″ is the wavelength for direct acceptor excitation. E does not depend on the percentage of acceptor-labeled molecules. We set $d^+ = 1$ because we used purified labeled oligos. We noticed a loss of acceptor emission during trinucleosome preparation, probably from photobleaching. This explains the larger-than-expected Cy3 donor emission[12].

Stopped-flow measurements. We used an Applied Photophysics instrument for the stopped-flow experiments, allowing analyses on timescales of 1 ms and longer. Cy3 was excited using an Argon arc lamp with a 500–530-nm bandpass filter, and we monitored Cy5 emission through a 650-nm cut-on filter. Trinucleosomes and $MgCl_2$ were separately diluted into 5 mM Tris, pH8.0, and mixed at 1:1 (v/v) ratio. Final concentrations were 25 nM, 10 nM and 1.5 nM trinucleosomes and 0 mM, 0.5 mM and 1mM $MgCl_2$. We acquired Cy5 fluorescence emission intensity data on a log(time) scale from 1 ms to 100s. For experiments with 0.5 mM or 1 mM $MgCl_2$ concentrations, the fluorescence intensity at time = 0, F_0, is obtained from parallel reactions in which the nucleosomes are mixed with 0 mM $MgCl_2$ instead.

Fluorescence correlation spectroscopy measurements. We used a Zeiss Confocor 3 instrument for free-solution FCS experiments. We acquired donor (Alexa568) correlation functions for Alexa568/Alexa647 double-labeled (DNA mp34) and A568 donor only–labeled (DNA mp35) trinucleosome arrays. Fluctuations in donor fluorescence emission arise from both diffusion and from conformational fluctuations causing changes in FRET, and are described by the correlation function[13,48–51]:

$$G(t)_{\text{donor\&acceptor}} = \frac{\left(1+\frac{k_{bq}}{k_{qb}}\exp(-\lambda\tau)\right)}{\langle N\rangle\left(1+\frac{t}{\tau}\right)\left(1+\alpha^2\frac{t}{\tau}\right)^{1/2}}$$

$$= G(t)_{\text{donor-only}}\, x\left(1+\frac{k_{bq}}{k_{qb}}\exp(-\lambda\tau)\right) \quad (2)$$

Here, t is the lag time of the donor autocorrelation, τ the diffusion time, α the form factor of the confocal volume, N the average number of molecules in the confocal volume, k_{bq} and k_{qb} the forward and backward rates, respectively, between the bright and dark fluorescent states, and $\lambda = (k_{bq} + k_{qb})$. Diffusion is removed by taking the ratio of donor autocorrelation functions: $G(t)_{\text{donor\&acceptor}} / G(t)_{\text{donor-only}}$. This analysis requires that the translational diffusion coefficients of singly and doubly labeled arrays be identical. Although not strictly true, this is a good approximation, as translational diffusion coefficients are weak functions of molecular volume, and the additional fluorophore itself represents only a small increase in molecular volume. Alexa568 was excited using a 514.5-nm argon laser at 50 microwatts, and the emission isolated with a 530–590-nm bandpass filter. Samples contained 5 mM Tris, 10 mM DTT and 0 mM or 1 mM $MgCl_2$.

45. Feng, H.P., Scherl, D.S. & Widom, J. Lifetime of the histone octamer studied by continuous-flow quasielastic light scattering: test of a model for nucleosome transcription. *Biochemistry* **32**, 7824–7831 (1993).
46. Little, J.W. *et al.* Cleavage of LexA repressor. *Methods Enzymol.* **244**, 266–284 (1994).
47. Thåström, A., Lowary, P.T. & Widom, J. Measurement of histone-DNA interaction free energy in nucleosomes. *Methods* **33**, 33–44 (2004).
48. Bonnet, G., Krichevsky, O. & Libchaber, A. Kinetics of conformational fluctuations in DNA hairpin-loops. *Proc. Natl. Acad. Sci. USA* **95**, 8602–8606 (1998).
49. Krichevsky, O. & Bonnet, G. Fluorescence correlation spectroscopy: the technique and its applications. *Reports on Progress in Physics* (2002).
50. Hess, S.T., Huang, S., Heikal, A.A. & Webb, W. Biological and chemical applications of fluorescence correlation spectroscopy: a review. *Biochemistry* **41**, 697–705 (2002).
51. Elson, E.L. & Webb, W.W. Concentration correlation spectroscopy: a new biophysical probe based on occupation number fluctuations. *Annu. Rev. Biophys. Bioeng.* **4**, 311–334 (1975).

doi:10.1038/nsmb.1650